ELSEVIER

Journal of Organometallic Chemistry 527 (1997) 179–190

Journal of Organometallic Chemistry

Synthesis and redox chemistry of 1,1′-bis(diphenylphosphino)ferrocene derivatives of $R_2C_2Co_2(CO)_6$ ($R = MeO_2C$, CF_3)

C. John McAdam, Noel W. Duffy, Brian H. Robinson *, Jim Simpson

Department of Chemistry, University of Otago, PO Box 56, Dunedin, New Zealand

Received 31 May 1996

Abstract

$Fe(C_5H_4PPh_2)_2$ (dppf) undergoes facile thermal substitution reactions with $R_2C_2Co_2(CO)_6$ ($R = MeO_2C$, CF_3) to yield a variety of products. When $R = MeO_2C$, initial coordination gives μ^2-$(MeO_2C)_2C_2Co_2(CO)_5(\eta^1$-dppf); its crystal and molecular structure, monoclinic, $P2_1/c$, $a = 8.954(3)$, $b = 20.211(2)$ $c = 23.836(5)$ Å, $\beta = 100.55(2)°$, $Z = 4$, $R1 = 0.0345$ for 5764 reflections $I > 2\sigma(I)$, confirms the monodentate coordination mode for dppf. At low dppf/alkyne-complex ratios, oligomeric products with dppf ligands linking up to five (μ^2-$MeO_2C)_2C_2Co_2$ modules have been characterised but, as the proportion of the phosphine ligand increases, unstable products, which include a η^1-μ-η^1 dppf configuration, are obtained as well. In contrast, for $R = CF_3$, only $[(CF_3)_2C_2]Co_2(CO)_4(\eta^2$-dppf) is found in significant yield. A molecule with two different reduction centres, [μ^2-$(MeO_2C)_2C_2Co_2(CO)_5$](μ-dppf)[$Co_3(\mu^3$-CPh)$(CO)_8$], was also characterised. Electrochemistry of the dppf complexes was characterised by fast ligand dissociation upon reduction of the (μ-alkyne)Co_2 redox centre and oxidation of coordinated dppf. There was no evidence for communication between redox centres.

Keywords: Electrochemistry; Cobalt; Carboryl; X-ray structure; Ferrocenylphosphine

1. Introduction

The ligand 1,1′-bis(diphenylphosphino)ferrocene (dppf) exhibits considerable coordination diversity. In reactions with a wide variety of mononuclear transition metal systems the ligand has been observed to coordinate in a monodentate η^1 fashion [1,2], most commonly as a bidentate chelate ligand, η^2 [3–5] or as a link, η^1-μ-η^1 between two metal centres [6]. Polymeric compounds of this genre have also been characterised [7] and the additional involvement of the Fe atom in ancillary binding to a coordinated metal has been reported recently for complexes such as $[(dppf)Pd(PPh_3)_2](BF_4)_2$ [8]. Investigations of dppf ligation to multinuclear metal complexes are less common, but with metal carbonyl clusters there is a preference for edge bridging, μ-η^2, coordination [8,9]. Nevertheless, coordination of dppf in $PhCCo_3(CO)_7$(μ-η^2-dppf) [10] occurs on the axial face of the cobalt triangle away from the apical carbon atom, in contrast to the more common equatorial disposition favoured by bidentate ligands such as dppm and dppe [11]. Examples of both bridging, η^1 [12] and linked η^1-μ-η^1 clusters [13] have been reported, but the dinuclear complex $HW_2(CO)_9NO$ binds dppf in both the η^1 and μ-η^2 modes [14].

As a continuation of our study of the degree of communication between redox-active clusters linked by unsaturated or saturated spacers [15,16], we were interested to know whether the dppf ligand would mediate communication between two linked (μ^2-C_2)Co_2 or (μ^2-C_2)Co_2/(μ^3-C)Co_3-linked redox centres. Facile oxidation reactions have been observed for complexes containing the dppf ligand [17]. Coordination of one or more dppf ligands to a (μ^2-C_2)Co_2 module should increase the electron density on the Co_2C_2 core [18,19] and facilitate the oxidation of the cobalt centre. This would result in multiple redox centre systems with one or more oxidisable ferrocene centres together with an oxidisable cobalt centre in the same molecule [20,21]. This paper reports the isolation, characterisation and redox chemistry of compounds resulting from the reaction of dppf with $R_2C_2Co_2(CO)_6$, ($R = MeO_2C$, CF_3).

* Corresponding authors.

PII S0022-328X(96)06590-4

2. Results and discussion

The initial product of the substitution reaction between [μ^2-$(MeO_2C)_2C_2$]$Co_2(CO)_6$ and dppf at ambient temperature was the blood-red monosubstituted complex [μ^2-$(MeO_2C)_2C_2$]$Co_2(CO)_5(\eta^1$ dppf), **1**.

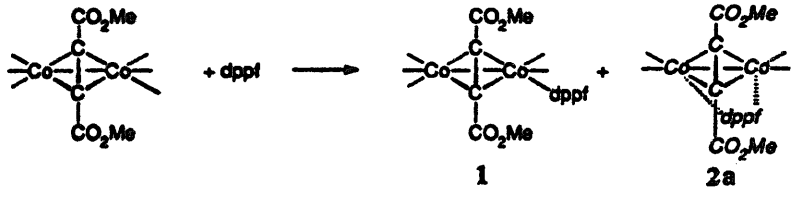

(1)

The labile μ-η^2 product, **2a** was only obtained in low yield. The availability of an uncoordinated pendant P-donor atom in **1** provides the template for oligomerisation and/or linked η^1-μ-η^1 dppf derivatives. Thus, further reaction with equimolar **1** and [μ^2-$(MeO_2C)_2C_2$]$Co_2(CO)_6$ gave **3a** in which two (μ^2-C_2)Co_2 modules are coupled by a η^1-μ-η^1 link (Eq. (2)).

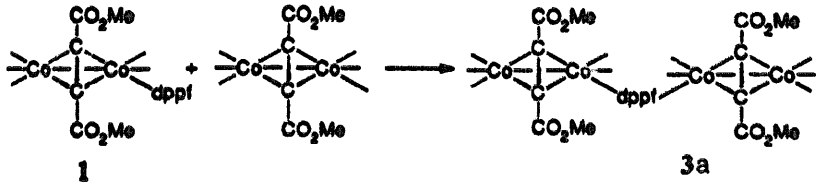

(2)

Similarly, the reaction of **1** with $PhCCo_3(CO)_9$ at 70 °C coupled (μ^2-C_2)Co_2 and (μ^3-C)Co_3 modules to give **11** (Eq. (3)) accompanied by low yields of **12**.

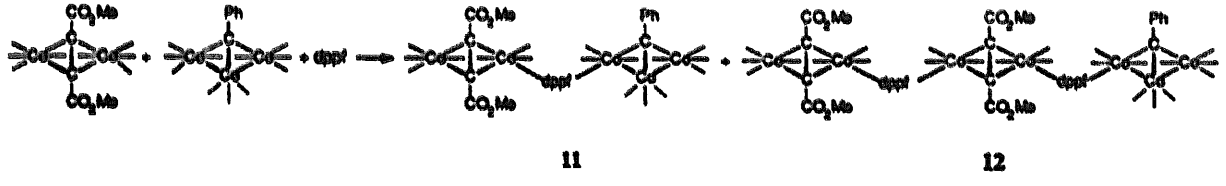

(3)

Reactions at elevated temperatures were dependent on both the ratio of the ligand to the [μ^2-$(MeO_2C)_2C_2$]Co_2 substrate and on the reaction temperature. Reactant ratios of 1:1 and temperatures up to 70 °C yielded principally **1** and **3a**. Significant yields of the higher, dppf-linked oligomers **4–6** were obtained, at the expense of **1**, at higher temperatures and with longer reaction times (Eq. (4)).

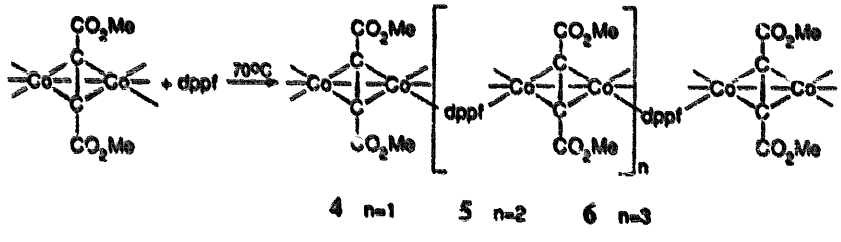

(4)

Similar reactions using an excess of the dppf ligand again produced **1–3a** at temperatures up to 70 °C. Reactions above 70 °C produced a different, and significantly more labile, product mix (**7–10**) in which compounds with both μ-η^2- and η^1-coordination of the dppf ligand (**8–10**) predominated (Eq. (5)).

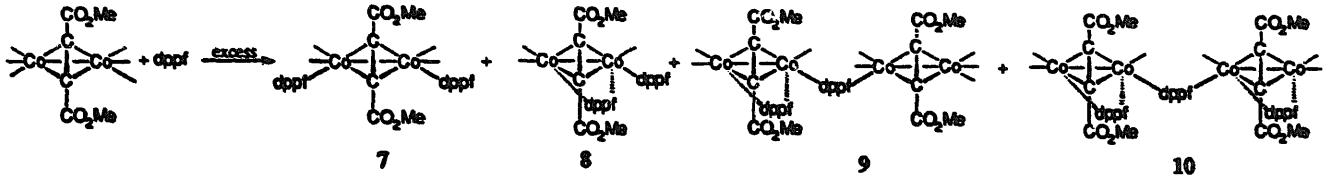

(5)

Compound **7**, in which each cobalt atom of a (μ^2-C_2)Co_2 complex carries an η^1-coordinated dppf ligand, and thus has dangling P available for additional coordination at both ends of the molecule, was a minor product of these high temperature reactions. Clearly this labile compound is an important intermediate in the formation of the higher oligomeric products.

The η^1-complex **1**, the η^1-μ-η^1-bridged oligomers **3a–6**, **11–12** are blood red to black solids, soluble in halogenated and aromatic solvents, acetone or ether, but insoluble in hexane. These compounds are all stable indefinitely in the solid state but decompose slowly in solution. In contrast, compounds **2a**, **8**, **9**, and **10**, which feature μ-η^2-coordination of the dppf ligand, are unstable in solution. Of these products only **2a** has been isolated in crystalline form.

Surprisingly, reactions of dppf with μ^2-$(CF_3)_2C_2Co_2(CO)_6$ gave **2b** as the dominant product; **3b** was a minor product with only traces of other η^1 or η^2 complexes. The apparent instability of complexes with pendant P-donor atoms explains why oligomers do not feature in reactions with [μ^2-$(CF_3)_2C_2$]$Co_2(CO)_6$.

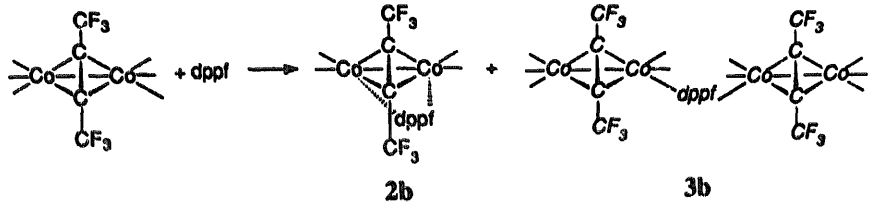

(6)

2.1. Characterisation and structure determination

All complexes have been characterised by ^{1}H and ^{31}P NMR and IR spectroscopy. However, the solid-state structure of **1** will be described first as it provides a template for the identification of the likely coordination preferences for the oligomeric η^1-μ-η^1-bridged derivatives.

2.2. X-ray crystal structure of [μ^2-$(MeO_2C)_2C_2$]$Co_2(CO)_5$[$(Ph_2PC_5H_4)Fe(C_5H_4PPh_2)$], 1

Selected bond length and angle data for **1** are given in Table 1 and a perspective view of the molecule in Fig. 1 defines the atom numbering scheme. The molecule consists of a typical, tetrahedral (μ^2-C_2)Co_2 core with the alkyne carbon atoms C(3) and C(4) arranged approximately orthogonal to the Co(1)–Co(2) bond (interline angle 92.2°). The remaining carbonyl ligands and the Co bound P(1) atom of the η^1-dppf ligand adopt a classical 'sawhorse' arrangement [22] with the pseudo-equatorial carbonyl ligands roughly eclipsed when viewed down the Co(1)–Co(2) vector. The coordination geometry about the Co atoms of these complexes is generally described as distorted octahedral [23] with the octahedra sharing a common face, defined in this structure by the carbyne carbon atoms C(3) and C(4) and the 'bent' Co–Co bond [24]. In **1**, the P(1) donor atom binds to a pseudoaxial site, which has been shown to be the site of coordination preference for a number of ligand species with poorer π-acceptor ability than CO [25]. The pendant P(2) atom of the dppf ligand is located well away from the remaining coordination sites on the Co atoms, and as such is available for intermolecular coordination to an alternative acceptor, vide supra. Bond lengths and angles within the dppf ligand fragment are unremarkable, and the two η^5-cyclopentadiene rings are almost parallel, a testament to the lack of strain in the η^1-coordination mode of the ligand in this molecule.

The Co(1)–Co(2) bond is 2.4749(7) Å long. This is in good agreement with the bond lengths observed for the parent hexacarbonyl (2.477(3) Å) [26] and for a disubstituted complex with both Me_3P ligands coordinated in

Table 1
Selected bond lengths (Å) and angles (deg) for 1

C(1)–O(1)	1.454(6)	O(1)–C(2)	1.322(5)
C(2)–O(2)	1.197(5)	C(2)–C(3)	1.467(5)
C(3)–C(4)	1.340(5)	C(4)–C(5)	1.467(5)
C(5)–O(5)	1.192(5)	C(5)–O(6)	1.330(5)
O(6)–C(6)	1.445(4)	C(3)–Co(1)	1.957(3)
C(4)–Co(1)	1.920(3)	C(3)–Co(2)	1.947(4)
C(4)–Co(2)	1.974(3)	Co(1)–Co(2)	2.4749(7)
Co(1)–P(1)	2.2237(9)	Co(1)–C(111)	1.797(4)
C(111)–O(111)	1.122(4)	Co(1)–C(112)	1.797(3)
C(112)–O(112)	1.134(4)	Co(2)–C(211)	1.803(5)
C(211)–O(211)	1.123(6)	Co(2)–C(212)	1.819(5)
C(212)–O(212)	1.114(6)	Co(2)–C(213)	1.813(5)
C(213)–O(213)	1.119(5)	P(1)–C(7)	1.828(3)
P(1)–C(13)	1.826(3)	P(1)–C(19)	1.810(3)
C(19)–C(20)	1.429(4)	C(19)–C(23)	1.433(4)
C(20)–C(21)	1.416(5)	C(21)–C(22)	1.401(5)
C(22)–C(23)	1.426(5)	C(24)–C(25)	1.429(5)
C(24)–C(28)	1.424(5)	C(24)–P(2)	1.828(3)
C(25)–C(26)	1.419(5)	C(26)–C(27)	1.403(5)
C(27)–C(28)	1.404(5)	P(2)–C(29)	1.829(3)
P(2)–C(35)	1.832(4)		
C(4)–C(3)–C(2)	141.3(4)	C(3)–C(4)–C(5)	140.5(3)
C(111)–Co(1)–P(1)	95.57(11)	C(112)–Co(1)–P(1)	99.42(11)
C(112)–Co(1)–C(111)	107.4(2)	C(3)–Co(1)–P(1)	104.13(10)
C(4)–Co(1)–P(1)	104.09(11)	P(1)–Co(1)–Co(2)	152.90(3)
C(111)–Co(1)–Co(2)	99.43(11)	C(112)–Co(1)–Co(2)	97.47(11)
C(211)–Co(2)–C(212)	99.4(2)	C(211)–Co(2)–C(213)	101.6(2)
C(213)–Co(2)–C(212)	106.1(3)	C(211)–Co(2)–Co(1)	144.9(2)
C(212)–Co(2)–Co(1)	102.1(2)	C(213)–Co(2)–Co(1)	98.6(2)
O(111)–C(111)–Co(1)	177.3(3)	O(112)–C(112)–Co(1)	175.0(3)
O(211)–C(211)–Co(2)	174.8(5)	O(212)–C(212)–Co(2)	178.4(6)
O(213)–C(213)–Co(2)	177.0(4)	C(13)–P(1)–C(7)	104.42(13)
C(19)–P(1)–C(7)	104.34(14)	C(19)–P(1)–C(13)	101.39(14)
C(20)–C(19)–P(1)	126.2(2)	C(23)–C(19)–P(1)	126.2(2)
C(25)–C(24)–P(2)	125.0(3)	C(28)–C(24)–P(2)	128.2(3)
C(24)–P(2)–C(29)	102.5(2)	C(24)–P(2)–C(35)	99.5(2)
C(29)–P(2)–C(35)	100.9(2)		

pseudo-axial sites (Co–Co 2.464(1) Å) [27]. The monodentate coordination observed here to a pseudoaxial coordination position ensures a relatively uncluttered steric environment. This is reflected in the separation of the Co atoms. Extension of the Co–Co bond beyond 2.500 Å has been observed in (μ_2-C_2)Co_2 systems where the bidentate phosphine or arsine ligands either chelate to a single metal (η^2-coordination) [28] or bridge the metal–metal bond in a in μ-η^2 fashion [29]; this has been ascribed to steric demands of the non-carbonyl ligands. It is interesting that no such extension is observed on μ-η^2 coordination of the biphosphine ligand, P_2Ph_4, to a μ-alkynedicobalt system [30], again suggesting that the extension is based on the steric requirements of the ligand system.

2.3. Spectroscopic data

The progenitor of **2a–10**, complex **1**, is spectroscopically characterised by a typical three-band ν(CO) spectrum for coordination of the phosphine substituent in a pseudo-axial position and the required integrated intensities in the ^{1}H and ^{31}P NMR spectrum with coordinated and uncoordinated ^{31}P resonances at 43.5 and −17.4 ppm respectively. Essentially identical spectra are displayed by **3a**, strongly indicating that coordination of both P atoms is at a pseudo-axial site. For the related complex, **7**, the ν(CO) spectrum of three strong bands is shifted to lower frequencies by 30–40 cm^{-1}, in response to the replacement of a second CO ligand by the poorer π-accepting phosphine. The profile of this spectrum is similar to that of $R_2C_2Co_2(CO)_4L_2$ [23], where 1,1′-diaxial substitution is again the preferred option [25]. Linking of the (μ_2-C_2)Co_2 modules by dppf results in products with two discrete types of carbonyl substitution. The 'outer' μ^2-$(MeO_2C)_2C_2Co_2(CO)_5$ moieties in **3a** and at the end of the oligomeric chains in **4–6** should show identical spectra to that of **1**, while the spectrum of the 'inner' (μ^2-$MeO_2C)_2C_2Co_2(CO)_4$ fragments should mimic that of **7**. Consequently, the overall spectra of **4–8** are effectively composites of these two components giving a series of four-band ν(CO) spectra. Similarly the ν(CO) spectrum of **9**, which has two dppf

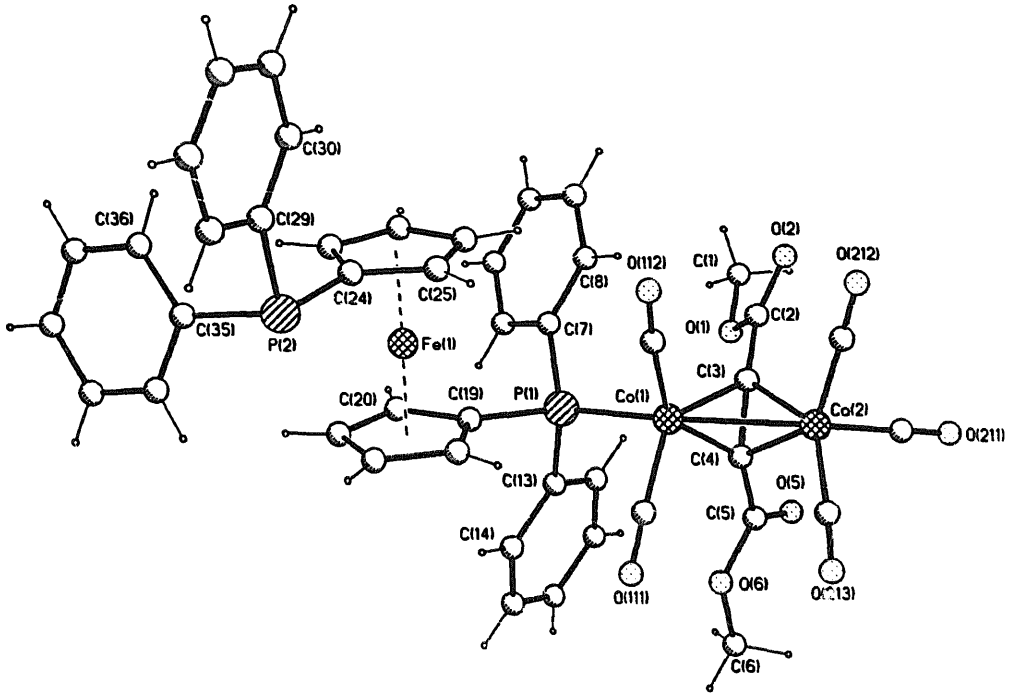

Fig. 1. Perspective view of **1** showing the atom numbering scheme.

ligands coordinated μ-η^2 and η^1, is the sum of **8** and **1**, while the similar CO coordination environments of **10** and **8** is reflected in their spectra. In keeping with this theme, ν(CO) for **11** is the sum of **1** and ν(CO) for a (μ^3-CPh)$Co_3(CO)_8P$ derivative with the ligand in an equatorial position [31].

Comparison of the chemical shift data and integration of the ^1H and ^{31}P resonances for compounds **1–10** provide identification, particularly for the oligomeric series **3a–6** where the relative intensities of the methoxy proton resonances and those of the coordinated P atoms give the ratio of 'outer' to 'inner' Co_2 units with extension of the oligomeric chain. Note that the chemical shifts of the 'inner' P atoms are consistently to high field of the P-atoms coordinated to the 'outer' Co_2 units. For the hexafluorobut-2-yne complexes the loss of proton resonances from the (μ_2-C_2)Co_2 moiety removes the internal standard, but a combination of multinuclear NMR and IR data allow effective characterisation of these compounds.

2.4. Electrochemistry

Any interpretation of the electrochemistry of these complexes needs to take into account the redox activity of the ligand dppf [17,32]. For dppf, one-electron oxidation of the ferrocenyl centre (E° = 0.183 V vs. Fc^+/Fc) to $dppf^+$ is followed by fast chemical reactions at ambient temperature. Intramolecular electron transfer is believed to give a phosphinium radical ion which subsequently dimerises and/or reacts with water to give protonated and oxide species which are also redox-active.

Coordination of dppf to a heavy transition metal ion (e.g. Pt[II]) usually simplifies the responses associated with the ferrocenyl couple, but ligand dissociation leads to more complex electrochemistry for most other complexes [33].

At temperatures below −15 °C (Fig. 2(a)) **1** has a relatively simple electrochemistry. The uncomplicated reversible one-electron oxidation process **X** at $E_{1/2}$ = 0.85 V (I_p^c/I_p^a = 1) can be assigned to the Fc/Fc^+ couple for the coordinated dppf; it is at a similar potential to that for $[Cu_2(dppf)_2(\mu\text{-dppf})]^{2+}$ [34] and $PhCCo_3(CO)_7(dppf)$ [10] but positive of $M(dppf)_2Cl_2$ (M = Pd[II], Pt[II]) at ca. 0.73 V [33]. A one-electron reduction couple **A** at $E_{1/2} \sim -1.07$ V, $I_p^a/I_p^c < 1$ (the exact ratio depends on switching potential and scan rate) is consistent [18,23] with the reduction of a (μ-C_2)$Co_2(CO)_5P$ moiety. The absence of chemical reversibility for **A** is observed with other (μ-alkyne)$Co_2(CO)_6$ derivatives — a fragmentation mechanism is involved [18,19] — which implies that oxidation of the dppf has no effect on the redox processes for the Co_2 module.

A further irreversible reduction process **C** occurs at ca. −1.4 V. **C**, a feature found in all complexes, has a potential consistent with the formation of a radical anion with *two* phosphorus donors *per* $Co_2(CO)_x$ module [18,23]. The scan rate dependency, CO-dependence and link with the formation of **A**, suggests that **C** is the result of an ECE process resulting in the formation of a chelated derivative which is partially stable on the electrochemical timescale. The identity of **C** could not be confirmed by other techniques because **2** is unstable in bulk solution. Stability at an

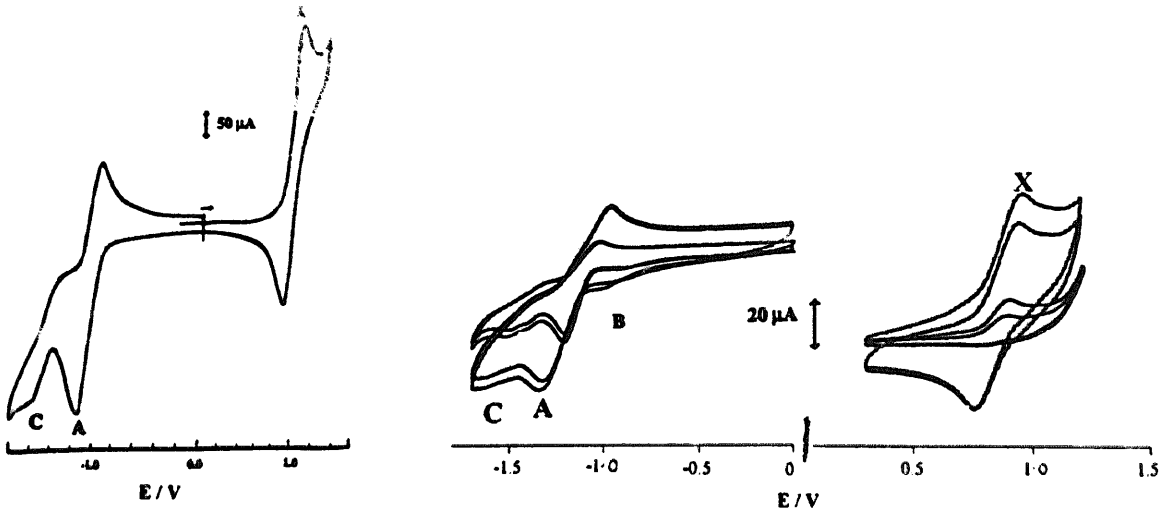

Fig. 2. (a) Cyclic voltammogram of **1** (1×10^{-3} M) at −15 °C; CH_2Cl_2, Pt, TEAP (0.1 M) vs. SCE, 200 mV s^{-1}. (b) As for (a) at −6 °C but on GCE and **1**, 200 mV s^{-1}, **2**, 1 V s^{-1}.

electrode surface but instability away from the interface is not unusual in metal carbonyl systems [18,35], a phenomenon we intend to explore by AFM methods. However, this assignment is supported by the cyclic voltammetry of **2b** which shows (Fig. 3) a reversible couple **C** with a cathodic shift compared with **C** in **1–10** expected because of the superior electron-withdrawing properties of CF_3. In common with other systems the ECE processes are slower for the CF_3 complexes, oxidation of coordinated dppf is chemically reversible at all sweep rates, and $\mathbf{2b}^{+\cdot}/\mathbf{2b}^{-\cdot}$ have a finite lifetime at ambient temperatures.

Above −15 °C both **X** and **A** become progressively more irreversible, **C** becomes more prominent and the *i–E* profiles are dependent on the scanning direction and scan rate (Fig. 2(b)). Initial scans at 200 mV s^{-1} in the anodic direction have $I_p^c/I_p^a \ll 1$ for **X** but $I_p^c/I_p^a \approx 1$ at 1 V s^{-1} providing the scan is switched 0.0 V; multiple scans in the full potential range show that **X**, **A** and **C**; however, **A** and **C** gradually disappear from the back scans. Conversely, cathodic scans show **A** and **C** which are more reversible at fast scan rates if **X** is not included in the back scan. The cyclic voltammetric response in the presence of CO is similar, the only difference being the appearance of an anodic wave due to $Co(CO)_4^-$ and the growth of a new cathodic wave **B** at the expense of **C**. **B**, which is also a common feature for all complexes on Pt if scans are greater than 1.0 V, has a potential which is not consistent with the reduction of a phosphine-substituted Co_2 complex; its current function increases under CO, its current profile is often that of an adsorbed species and, as it is cathodic of the reduction of $dppfH^+$, it is most likely due to a monomeric cobalt species [18]. Clearly, oxidation of dppf at greater than −15 °C leads to fast ligand dissociation and decomposition of the alkyne complex, a result found for other low valent dppf complexes [33].

$$< -15\,^{\circ}C \qquad \mathbf{1}^+ + e^- \leftrightarrow \mathbf{1} + e^- \leftrightarrow \mathbf{1}^- \rightarrow \mathbf{2}^-$$

$$> -15\,^{\circ}C \quad \text{decomp} \leftarrow \text{dppf}^+ \leftarrow \mathbf{1}^+ + e^- \leftrightarrow \mathbf{1} + e^- \leftrightarrow \mathbf{1}^- \rightarrow \mathbf{2}^- + \text{fragmentation}$$

Once dppf links to one or more $[(\mu^2\text{-}MeO_2C)_2C_2]Co_2(CO)_x$ modules the fast EC processes consequential upon oxidation or reduction dominate. In particular, the electrochemical profiles are dependent on whether the initial scan

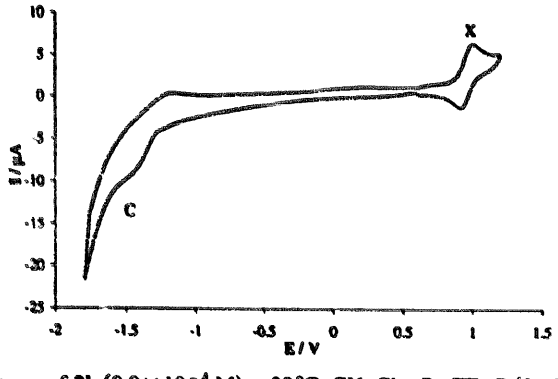

Fig. 3. Cyclic voltammogram of **2b** (0.9×10^{-4} M) at 20 °C; CH_2Cl_2, Pt, TEAP (0.1 M) vs. SCE, 500 mV s^{-1}.

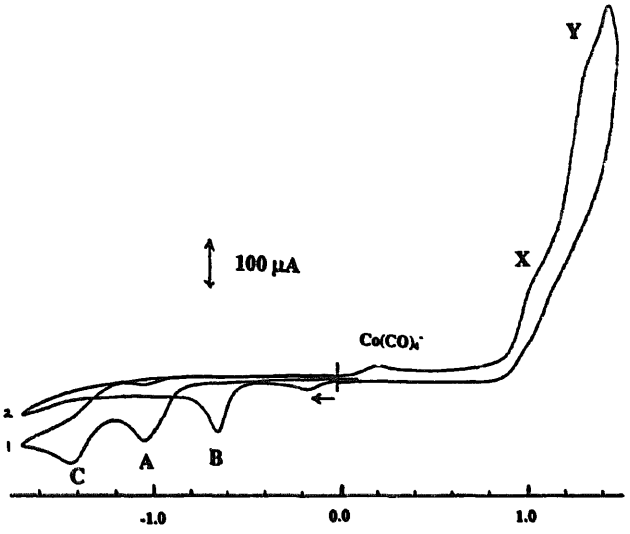

Fig. 4. Cyclic voltammogram of **3a** (1.0×10^{-3} M) at 20°C; CH_2Cl_2, Pt, TEAP (0.1 M) vs. SCE, 500 mV s^{-1}.

direction is anodic or cathodic. Nevertheless, there is a remarkable similarity between the *i* vs. *V* responses for all the complexes **3a** → **10**. Typical results are given in Fig. 4 for the linked complex with two Co_2 modules, **3a**. The first oxidation process **X** in an anodic scan corresponds to that for complex **1**; likewise, with an initial cathod c sweep the reduction wave profiles (**A** and **C**), and their potentials are virtually identical to those for **1**.

A consistency of electrochemical profile and potentials for **3a** → **10** indicates that for all these complexes the formation of a radical anion results in the fast dissociation of the Co–dppf bonds leading eventually to the same sequence of ECE reactions as those for **1**. In the electrochemistry of **3a** → **10** there is a second irreversible oxidation process **Y** at ca. 1.3 V. The ratio $i(X/Y)$ is always less than 0.5 and is markedly dependent on scan rate, complex and electrode; it is not an oxidation process of the free dppf ligand. Although irreversible oxidation of (μ^2-alkyne)$Co_2(CO)_6PR_3$ complexes has been noted previously in the potential range 1.1–1.5 V [23], this assignment is unlikely given the high currents and the absence of this oxidation in **1**. Couple **A** is lost on repeat scans if **Y** is included, and **B** is the only reduction wave observed.

Molecule **11** has one end of the Co_2dppf chain anchored by a redox-active $RCCo_3(CO)_8$ unit, a unit which undergoes similar, but slower, ECE reactions to the $Co_2(CO)_x$ module [36]. The anodic scan is similar to those for **3a** → **10** and **A**/**C** are again found in an initial cathodic scan (Fig. 5). An additional couple **D** at $E_p = -0.82$ V, nearly chemically reversible at low temperatures, is at a typical potential for $RCCo_3(CO)_8L$ derivatives and can be assigned to the formation of the 49e$^-$ radical anion $RCCo_3(CO)_8P^{\cdot-}$. Other waves on the reverse reduction scans are typical of those produced from ECE reactions involving $RCCo_3(CO)_8P^{\cdot-}$, especially the oxidation of $Co(CO)_4^-$.

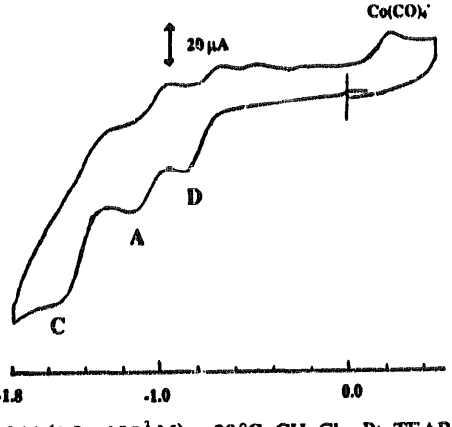

Fig. 5. Cyclic voltammogram of **11** (1.0×10^{-3} M) at 20°C; CH_2Cl_2, Pt, TEAP (0.1 M) vs. SCE, 200 mV s^{-1}.

Clearly, the two redox centres in **11** are acting independently, and cleavage of the μ-dppf bridges is again the dominant reaction upon oxidation or reduction.

3. Conclusion

Dppf reactions with $R_2C_2Co_2(CO)_6$ were surprisingly dependent on the substituent on the alkyne, those for $R = MeO_2C$ being based on the formation of an η^1 derivative followed by oligomerisation, whereas when $R = CF_3$ an η^2 binding mode spanning the metal–metal bond dominates. An explanation is not immediately obvious as they track one another in reactions with dppm or PR_3, and in their electrochemistry; they have similar steric requirements and are both electron-withdrawing alkyne substituents. The redox activity of both the $(\mu^2\text{-}C_2)Co_2$ and dppf components in these modules make them unsuitable for incorporation as conducting links in molecular wires.

4. Experimental

All reactions were carried out under an inert atmosphere. The complexes $R_2C_2Co_2(CO)_6$ [37], $Co_3(\mu^3\text{-CPh})(CO)_9$ [38] and $[C_5H_4PPh_2]_2Fe$ [39] were prepared by published procedures. All solvents were dried by standard methods. NMR and IR spectra were recorded on a Varian 300VXR and Digilab FTIR spectrometers respectively. ^{31}P NMR spectra were referenced to external H_3PO_4. Microanalyses were carried out by the Campbell Microanalytical Laboratory, University of Otago. FAB mass spectra were recorded on a Kratos MS80RFA with Iontech FABgun ZN11F at the University of Canterbury. All electrochemistry was carried out in dry solvents under N_2 atmosphere. A three-electrode cell equipped with a Luggin capillary was used for all measurements. The best results were obtained with a Pt-disc or glassy carbon electrode (GCE) with a saturated calomel electrode (SCE) referenced against the Fc/Fc^+ couple at $E_{1/2} = 0.505$ V. Solutions were typically 10^{-3} M in (0.1 M TEAP) acetone.

4.1. Reactions of dppf with $[(\mu^2\text{-}MeO_2C)_2C_2]Co_2(CO)_6$

4.1.1. 1:1 mole ratio

Dppf (260 mg, 0.47 mmol) was added to $[(\mu^2\text{-}MeO_2C)_2C_2]Co_2(CO)_6$ (200 mg, 0.47 mmol) in dry N_2 flushed toluene (50 cm^3). The reaction was followed by TLC as the solution changed colour from red-orange to a dark red. The first product to form in all cases was $[\mu^2\text{-}(MeO_2C)_2C_2]Co_2(CO)_5(\eta^1\text{-dppf})$, **1**, isolated by removing the solvent under reduced pressure followed by separation on preparative TLC silica plates with dichloromethane ($R_f = 0.5$). Recrystallisation from CH_2Cl_2 layered with hexane yielded blood-red crystals of **1** in yields of up to 54% (240 mg). Anal. Found: C, 56.15; H, 3.80; P, 6.52. $C_{45}H_{34}Co_2FeO_9P_2$. Calc.: C, 56.63; H, 3.59; P, 6.49%. Mass spectrum: *m/e* 954 (M^+), 830 ($MO^+ - 5CO$). ^1H NMR ($CDCl_3$): δ 3.34 (6H, s, $-OCH_3$); 3.68, 3.95, 4.23, 4.41 (8H, Fc-*H*); 7.2–7.4 (20 H, m, $-PPh_2$). ^{31}P NMR ($CDCl_3$): $\delta = 17.4$ ($-PPh_2$); 43.5 ($Co-PPh_2$). IR (CH_2Cl_2): ν_{CO} 2077 (s), 2028 (vs), 1984 (mw) cm^{-1}.

Yields of the other products were dependent on reaction temperature and time, but the general separation procedure was to remove the solvent under reduced pressure and separate using preparative TLC silica plates with a CH_2Cl_2:Et_2O (20:1) solvent mixture. Reaction at room temperature gave predominantly two products, a typical 2 h reaction yielding unreacted dicobalt complex (34 mg), **1** (136 mg, 31% yield), and **3a** (78 mg, 25% yield). Reaction at elevated temperature led to a large number of other products. Typically, chromatography of a mixture reacted at 70 °C for 1 h, produced the following major products. Band (2), $R_f = 0.7$, green-brown, crystallised from CH_2Cl_2 layered with MeOH to give small black crystals of **2**, 9 mg. Anal. Found: C, 57.35; H, 3.60; P, 7.06. $C_{44}H_{34}Co_2FeO_8P_2$. Calc.: C, 57.05; H, 3.70; P, 6.69%. Mass spectrum: *m/e* 926 (M^+). ^1H NMR ($CDCl_3$); δ 3.30 (6H, s, $-OCH_3$); 3.69, 4.05, 4.42, 5.07 (8H, Fc-*H*); 7.2–8.0 (20 H, m, $-PPh_2$). ^{31}P NMR: ($CDCl_3$) δ 44.2 ($Co-PPh_2$). IR (CH_2Cl_2): ν_{CO} 2057 (s), 2025 (m), 2004 (vs), 1962 (mw) cm^{-1}. Band (3), $R_f = 0.53$ blood-red **3a**, 107 mg. Anal. Found: C, 49.00; H, 3.23; P, 4.54. $C_{56}H_{40}Co_4FeO_{18}P_2$. Calc.: C, 49.66; H, 2.98; P, 4.57%. Mass spectrum: *m/e* 1354 (M^+). ^1H NMR ($CDCl_3$): δ 3.34 (12H, s, $-OCH_3$); 4.02 (8H, m, Fc-*H*); 7.25–7.45 (20H, m, $-PPh_2$). ^{31}P NMR ($CDCl_3$): δ43.0 ($Co-PPh_2$). IR (CH_2Cl_2): ν_{CO} 2078 (s), 2029 (vs), 1983 (mw) cm^{-1}. Band (4), $R_f = 0.47$, blood red, **4**, 25 mg. Anal. Found: C, 52.88; H, 3.52; P, 5.40. $C_{100}H_{74}Co_6Fe_2O_{26}P_4$. Calc.: C, 52.66; H, 3.27; P, 5.43%. ^1H NMR ($CDCl_3$): δ 2.73 (6H, s, $-OCH_3$); 3.33 (12H, s, $-OCH_3$); 4.0 (16H, m, Fc-*H*); 7.1–7.4 (40H, m, $-PPh_2$). ^{31}P NMR ($CDCl_3$): δ 41.5 (2P, $P-Co_2(Co)_4-P$); 43.2 (2P, $P-Co_2(CO)_5$). IR (CH_2Cl_2): ν_{CO} 2077(s), 2030 (vs), 1997 (m), 1978 (m) cm^{-1}. Band (5) $R_f = 0.2$, as a dark red powder from CH_2Cl_2–MeOH, **5**, 25 mg. Anal. Found: C, 54.17; H, 3.15; P, 5.96. $C_{144}H_{108}Co_8Fe_3O_{34}P_6$; Calc.: C, 53.93; H, 3.39; P, 5.79%. ^1H NMR ($CDCl_3$): δ 2.72 (12H, s, $-OCH_3$); 3.33 (12H, s, $-OCH_3$); 3.9–4.0 (24H, m, Fc-*H*); 7.1–7.4 (60H, m, $-PPh_2$). ^{31}P NMR ($CDCl_3$): δ 41.5 (4P, $P-Co_2(CO)_4-P$); 43.2 (2P, $P-Co_2(CO)_5$). IR (CH_2Cl_2): ν_{CO} 2077 (s), 2030 (vs), 1998 (m), 1976 (m) cm^{-1}. Band

(6), $R_f = 0.1$, dark red powder, **6** 7 mg. ^{1}H NMR ($CDCl_3$): δ 2.71 (18 H, s, $-OCH_3$); 3.32 (12H, s, $-OCH_3$); 3.9–4.0 (32H, m, Fc-*H*); 7.1–7.4 (80H, m, $-PPh_2$). ^{31}P NMR ($CDCl_3$): δ 41.5 (6P, *P*–$Co_2(CO)_4$–*P*); 43.2 (2P, *P*–$Co_2(CO)_5$). IR (CH_2Cl_2): ν_{CO} 2076 (s), 2031 (vs), 1998 (m), 1974 (m) cm^{-1}.

4.1.2. 3:1 mole ratio, dppf: $[\mu^2$-$(MeO_2C)_2C_2]Co_2(CO)_6$

Dppf (780 mg, 1.4 mmol) was added to $[\mu^2$-$MeO_2C)_2C_2]Co_2(CO)_6$ (200 mg, 0.47 mmol) in toluene. The first product was **1** but when held at 70 °C significant amounts of **2** and **3a** also formed. On raising the reaction temperature to 90 °C, a different mixture of products was obtained which were separated using preparative silica plates, CH_2Cl_2:Et_2O (20:1). A typical reaction yielded: Band (1) $R_f = 1.0$, yellow (220 mg) unreacted dppf; Band (2), $R_f = 0.7$, blood red, **7**, 8 mg. Anal. Found: C, 63.49; H, 4.68; P, 8.83. $C_{78}H_{62}Co_2Fe_2O_8P_4$. Calc.: C, 63.27; H, 4.22; P, 8.37%. ^{1}H NMR ($CDCl_3$): δ 2.75 (6H, s, $-OCH_3$); 3.63, 3.93, 4.24, 4.35 (16H, Fc-*H*); 7.1–7.3 (40H, m, $-PPh_2$). ^{31}P NMR ($CDCl_3$): δ −17.1 (2P, $-PPh_2$); 41.5 (2P, Co–PPh_2). IR (CH_2Cl_2): ν_{CO} 2034 (vs), 1996 (vs), 1971 (vs) cm^{-1}. Band (3), $R_f = 0.6$, brown, **8**, 430 mg, unstable in solution. Anal. Found: C, 63.55; H, 4.72; P, 8.41. $C_{77}H_{62}Co_2Fe_2O_7P_4$: Calc.: C, 63.66; H, 4.30; P, 8.53%. Mass spectrum: during run progressed from *m/e* 1368 ($M^+ - 3CO$) to peaks attributed to oxidised product *m/e* 1468 (MO^+), 1412 ($MO^+ - 2CO$), 1384 ($MO^+ - 3CO$). ^{1}H NMR ($CDCl_3$): δ 2.74 (6H, s, $-OCH_3$); 3.49, 3.73, 3.95, 4.17, 4.41, 5.30 (16H, Fc-*H*); 7.1–8.0 (40H, m, $-PPh_2$). ^{31}P NMR ($CDCl_3$): δ −17.1 (1P, $-PPh_2$); 32.7 (1P, t, $^3J_{P-P} = 50$ Hz); 42.0 (2P, broad). IR (CH_2Cl_2): ν_{CO} 2003 (s), 1960 (vs), 1931 (w) cm^{-1}. Band (4), $R_f = 0.34$, unstable in solution, brown, **9**, 37 mg. ^{1}H NMR ($CDCl_3$): δ 2.73 (6H, s, $-OCH_3$); 3.33 (6H, s, $-OCH_3$); 3.48, 3.73, 3.79, 3.81, 3.96, 4.42, 5.32 (16H, Fc-*H*); 7.1–8.0 (40H, m, $-PPh_2$). ^{31}P NMR ($CDCl_3$); δ 32.5 (1P, t, $^3J_{P-P} = 50$ Hz); 42.2 (2P, broad); 43.2 (1P, s). IR (CH_2Cl_2): ν_{CO} 2076 (s), 2029 (vs), 2007 (s), 1960 (s) cm^{-1}. Band (5), $R_f = 0.2$, brown, unstable in solution, **10**, 20 mg. ^{1}H NMR ($CDCl_3$): δ 2.70 (12H, s, $-OCH_3$); 3.47, 3.53, 3.65, 3.94, 4.40, 5.27 (24H, Fc-*H*); 7.0–8.0 (60H, m, $-PPh_2$). ^{31}P NMR ($CDCl_3$): δ 32.2 (2P, t, $^3J_{P-P} = 50$ Hz); 42.1 (4P, broad). IR (CH_2Cl_2): ν_{CO} 2006 (s), 1962 (vs), 1943 (w) cm^{-1}.

Table 2
Crystal data and structure refinement for **1**

Empirical formula	$C_{45}H_{34}Co_2FeO_9P_2$
Formula weight	954.37
Temperature (K)	294(2)
Wavelength (Å)	0.71073
Crystal system	Monoclinic
Space group	$P2_1/c$
Unit cell dimensions	
a (Å)	8.954(3)
b (Å)	20.211(2)
c (Å)	23.836(5)
α (deg)	90
β (deg)	100.5(2)
γ (deg)	90
Volume (Å^3)	4241(2)
Z	4
Density (calc.) (Mg m^3)	1.495
Absorption coefficient (mm^{-1})	1.241
F(000)	1944
Crystal size (mm^3)	0.4×0.2×0.15
θ range for data collection (deg)	2.01 to 24.98
Index ranges	$-10 \le h \le 10$, $-24 \le k \le 0$, $0 \le l \le 28$
Independent reflections	7411 ($R_{int} = 0.0314$)
Absorption correction	empirical
Transmission	0.99 (max)
	0.87 (max)
Refinement method	Full-matrix least squares on F^2
Data/parameters	7411/534
Goodness-of-fit on F^2	1.139
Final R indices ($I > 2\sigma(I)$)	$R1 = 0.0345$, $wR2 = 0.0847$
R indices (all data)	$R1 = 0.0547$, $wR2 = 0.1070$
Largest diff. peak and hole (e Å^{-3})	0.589 and −0.383

Table 3
Atomic coordinates ($\times 10^4$) and equivalent isotropic displacement parameters ($Å^2 \times 10^3$) for 1

	x	y	z	U_{eq}
C(1)	160(8)	799(4)	4101(3)	148(3)
O(1)	1108(4)	1240(2)	4498(1)	93(1)
C(2)	2582(5)	1124(2)	4559(2)	68(1)
O(2)	3126(5)	701(2)	4308(2)	107(1)
C(3)	3436(4)	1588(2)	4971(1)	54(1)
C(4)	3288(4)	1960(2)	5422(1)	51(1)
C(5)	2295(4)	2038(2)	5844(2)	61(1)
O(5)	1389(4)	1637(2)	5931(2)	103(1)
O(6)	2538(3)	2609(2)	6124(1)	73(1)
C(6)	1653(6)	2716(3)	6565(2)	95(2)
Co(1)	4439(1)	2446(1)	4955(1)	41(1)
Co(2)	5226(1)	1469(1)	5563(1)	62(1)
C(111)	5139(4)	3090(2)	5454(1)	50(1)
O(111)	5561(3)	3478(1)	5782(1)	72(1)
C(112)	5778(4)	2352(2)	4484(1)	51(1)
O(112)	6667(3)	2255(2)	4211(1)	77(1)
C(211)	4566(6)	762(2)	5909(2)	88(1)
O(211)	4048(6)	332(2)	6104(2)	137(2)
C(212)	6531(7)	1056(3)	5176(2)	96(2)
O(212)	7307(6)	805(3)	4927(2)	155(2)
C(213)	6398(6)	1886(2)	6159(2)	88(1)
O(213)	7083(5)	2168(2)	6521(2)	131(2)
P(1)	2717(1)	3072(1)	4407(1)	37(1)
C(7)	1640(3)	2698(2)	3759(1)	40(1)
C(8)	2237(3)	2166(2)	3510(1)	46(1)
C(9)	1440(4)	1887(2)	3011(1)	58(1)
C(10)	67(4)	2134(2)	2761(1)	59(1)
C(11)	−543(4)	2666(2)	3003(2)	60(1)
C(12)	242(3)	2946(2)	3499(1)	51(1)
C(13)	1268(3)	3358(2)	4799(1)	44(1)
C(14)	1363(4)	3981(2)	5047(2)	61(1)
C(15)	309(5)	4173(2)	5379(2)	81(1)
C(16)	−814(5)	3755(3)	5465(2)	82(1)
C(17)	−901(4)	3139(3)	5230(2)	80(1)
C(18)	126(4)	2929(2)	4891(2)	61(1)
C(19)	3396(3)	3848(2)	4169(1)	43(1)
C(20)	2535(4)	4304(2)	3780(1)	51(1)
C(21)	3408(4)	4887(2)	3770(2)	59(1)
C(22)	4802(4)	4800(2)	4139(2)	57(1)
C(23)	4816(4)	4160(2)	4394(1)	50(1)
Fe(1)	4513(1)	4078(1)	3524(1)	42(1)
C(24)	6105(4)	4252(2)	3028(1)	49(1)
C(25)	6376(4)	3637(2)	3326(2)	57(1)
C(26)	5092(4)	3226(2)	3152(2)	60(1)
C(27)	4021(5)	3581(2)	2763(2)	60(1)
C(28)	4634(4)	4206(2)	2682(1)	52(1)
P(2)	7382(1)	4965(1)	3130(1)	53(1)
C(29)	8689(4)	4785(2)	2643(1)	50(1)
C(30)	8540(4)	4268(2)	2260(2)	65(1)
C(31)	9609(5)	4167(2)	1917(2)	76(1)
C(32)	10801(5)	4588(2)	1937(2)	75(1)
C(33)	10968(4)	5105(2)	2308(2)	71(1)
C(34)	9919(4)	5206(2)	2665(2)	62(1)
C(35)	6146(4)	5584(2)	2717(2)	51(1)
C(36)	5787(4)	5589(2)	2124(2)	56(1)
C(37)	4763(4)	6033(2)	1835(2)	65(1)
C(38)	4070(5)	6489(2)	2130(2)	79(1)
C(39)	4439(6)	6501(2)	2714(2)	85(1)
C(40)	5457(5)	6053(2)	3005(2)	69(1)

U_{eq} is defined as one-third of the trace of the orthogonalized U_{ij} tensor.

4.1.3. Reaction of [μ^2-(MeO$_2$C)$_2$C$_2$]Co$_2$(CO)$_5$ (η^1-dppf) with Co$_3$(μ-CPh)(CO)$_9$

1 (57 mg, 0.06 mmol) was added to Co$_3$(μ^3-CPh)(CO)$_9$ (20 mg, 0.04 mmol) in 20 ml benzene and the reaction was followed using TLC. Stirring at 20 °C for 2 h led to preferential formation of **3a** and related compounds. Increasing the temperature to 70 °C resulted in the appearance of several darker bands on TLC. Solvent was removed under reduced pressure, and the reaction mixture separated using preparative TLC silica plates (CH_2Cl_2:Et_2O, 20:1). From the large number of products in the mixture, the derivatives **11** (13 mg, 23% yield) and **12** (7 mg, 10% yield) were characterised. **11**, (R_f = 0.9). Anal. Found: C, 49.33; H, 2.95; P, 4.51. $C_{60}H_{39}Co_5FeO_{17}P_2$. Calc.: C, 49.89; H, 2.72; P, 4.29%. Mass spectrum: *m/e* 1304 (M^+ − 5CO), 1080 (M^+ − 13CO). ^{1}H NMR ($CDCl_3$): δ 3.34 (6H, s, −OCH_3); 4.00 (8H, m, Fc-*H*); 7.1–7.4 (25H, m, phenyl-H). ^{31}P NMR ($CDCl_3$): δ 41.9 (1P, *P*–Co_3); 43.0 (1P, *P*–$Co_2(CO)_5$). IR (CH_2Cl_2); ν_{CO} 2077 (s), 2034 (vs), 2020 (vs), 2010 (m), 1987 (mw). **12**, (R_f = 0.8). ^{1}H NMR ($CDCl_3$): δ 2.72 (6H, s, −OCH_3); 3.33 (6H, s, −OCH_3); 3.9–4.05 (16H, m, Fc-H); 7.1–7.4 (45H, m, phenyl-H). ^{31}P NMR ($CDCl_3$): δ41.5 (2P, *P*–$Co_2(CO)_4$–*P*); 42.1 (1P, *P*–Co_3); 43.2 (1P, *P*–$Co_2(CO)_5$). IR (CH_2Cl_2): ν_{CO} 2077 (s), 2034 (vs), 2020 (vs), 2008 (s), 1979 (m).

4.1.4. Reaction of dppf with [μ^2-(CF$_3$)$_2$C$_2$]Co$_2$(CO)$_6$

To [μ^2-$(CF_3)_2C_2$]$Co_2(CO)_6$ (200 mg, 0.45 mmol) in dry N_2 flushed benzene was added dppf (200 mg, 0.36 mmol). No reaction was observed at ambient temperature, and the solution was heated to reflux (80 °C) for 2 h. The colour of the solution changed from red-orange to red-brown; solvent was removed under reduced pressure, and the reaction mixture separated using preparative TLC SiO_2 plates (CH_2Cl_2:hexane, 1:1) **2b**, (R_f = 0.58), crystallised from CH_2Cl_2 layered with MeOH, 83 mg (20%). Anal. Found: C, 52.73; H, 2.75; P, 6.53. $C_{42}H_{28}Co_2F_6FeO_4P_2$. Calc.: C, 53.31; H, 2.98; P, 6.55%. Mass spectrum: *m/e* 834 M^+ − 4CO. ^{1}H NMR ($CDCl_3$): δ 4.14 (4H, t, Fc-*H*); 4.36 (4H, m, Fc-*H*); 7.3–7.6 (20H, m, −PPh_2). ^{31}P NMR ($CDCl_3$): δ 35.2 (2P, −*P*Ph_2). IR (CH_2Cl_2): ν_{CO} 2049 (s), 2025 (vs), 2001 (s), 1972 (w) cm^{-1}. **3b**, (R_f = 0.64), yield 69 mg (22%). Mass spectrum: *m/e* 1254 (M^+ − 5CO), 1114 (M^+ − 10CO). ^{1}H NMR ($CDCl_3$): δ 3.92 (4H, m, Fc-*H*); 4.05 (4H, m, Fc-*H*); 7.2–7.5 (20H, m, −PPh_2). ^{31}P NMR ($CDCl_3$): δ 39.5 (2P, −*P*Ph_2). IR (CH_2Cl_2): ν_{CO} 2089 (s), 2042 (vs), 1994 (m) cm^{-1}.

4.1.5. X-ray data collection, reduction and structure solution for 1

A sample of **1** prepared as outlined above was recrystallised from CH_2Cl_2–hexane. A blood-red block was used for the data collection. Data were collected on a Nonius CAD4 diffractometer using graphite moderated Mo Kα radiation and the ω–2θ scan technique. Cell dimensions were derived from the angular measurements of 30 strong reflections in the range $3 < 2\theta < 14.5°$. Details of the crystals, data collection and structure refinement are summarised in Table 2. Lorentz and polarisation corrections were applied using locally written programs and absorption corrections were applied from empirical psi-scans [40]. The structure was solved by direct methods using SHELXS-86 [41]; the optimum electron density map revealed the location of the Fe, Co and P atoms together with the majority of the remaining C and O atoms. Remaining non-H atoms were located in subsequent difference Fourier, weighted full matrix least squares refinement cycles using SHELXL-93 [42]. Hydrogen atoms were included as fixed contributions to F_c with fixed isotropic temperature factors. All of the non-hydrogen atoms were refined anisotropically and this model of the structure converged with $R(\Sigma|F_o| - |F_c|/\Sigma|F_o|) = 0.0345$ ($F > 2\sigma F$, 5764 reflections), and $wR2 = [\Sigma w(F_o^2 - F_c^2)^2/\Sigma wF_o^4]^{1/2} = 0.1070$ (all data), $S = 1.139$, $w^1 = [^2(F_o^2) + (0.0426P)^2 + 3.79P$, and $P = (F_o^2 + 2F_c^2)/3$. The final difference Fourier map was essentially flat, with maxima at 0.59, and −0.38 e Å^{-3}. Final positional and equivalent thermal parameters are given in Table 3. A full listing of bond lengths and angles, thermal parameters, H atom parameters, observed and calculated structure factors and mean-plane data can be obtained from the authors (JS).

Acknowledgements

We thank Dr. C.E.F. Rickard, University of Auckland for the X-ray data collection, and Dr. B.M. Clark, University of Canterbury for the FAB mass spectra.

References

[1] F. Neuman and G. Suns-Fisk, *J. Organomet. Chem.*, *367* (1990) 175. T.S.A. Hor and L.T. Phang, *J. Organomet. Chem.*, *381* (1990) 121.
[2] T.J. Kim, K.H. Kwon, J.O. Baeg, S.C. Shim and D.H. Lee, *J. Organomet. Chem.*, *389* (1990) 205. H.S.O. Chan, T.S.A. Hor, L.T. Phang and K.L. Tan, *J. Organomet. Chem.*, *407* (1991) 353.
[3] I.R. Butler, W.R. Cullen, T.J. Kim, S.J. Rettig and J. Trotter, *Organometallics*, *4* (1985) 972. T.M. Miller, K.J. Ahmed and M.S. Wrighton, *Inorg. Chem.*, *28* (1989) 2347. S.A. Benyunes, L. Brandt, A. Fries, M. Green, M.F. Mahon and T.M.T. Papworth, *J. Chem. Soc. Dalton Trans.*, (1993) 3785. G. Pilloni, B. Corain, M. Degano, B. Longato and G. Zanotti, *J. Chem. Soc. Dalton Trans.*, (1993) 1777.

[4] V.C.M. Smith, R.T. Aplin, J.M. Brown, M.B. Hursthouse, A.I. Karalulov, K.M.A. Malik and N.A. Cooley, *J. Am. Chem. Soc., 116* (1994) 5180. T.F. Baumann, J.W. Sibert, M.M. Olmstead, A.G.M. Barrett and B.M. Hoffman, *J. Am. Chem. Soc., 116* (1994) 2639. A.L. Rheingold, B.S. Haggerty, A.J. Edwards, C.E. Housecroft, A.D. Hattersley and N. Hinze, *Acta Crystallogr. Sect. C:, 50* (1994) 411.
[5] S.P. Neo, Z.Y. Zhou, T.C.W. Mak and T.S.A. Hor, *J. Chem. Soc. Dalton Trans.*, (1994) 3451. G. Vasapollo, L. Toniolo, G. Cavinato, F. Bigoli, M. Lanfranchi and M.A. Pellinghelli, *J. Organomet. Chem., 481* (1994) 173. J.M. Brown, J.J. Perez-Torrente, N.W. Alcock and H.J. Clase, *Organometallics, 14* (1995) 207.
[6] M.C. Gimeno, A. Laguna, C. Sarroca and P.G. Jones, *Inorg. Chem., 32*, (1993) 5926; L.T. Phang, S.C.F. Au-Yeung, T.S.A. Hor, S.B. Khoo, Z.Y. Zhou and T.C.W. Mak, *J. Chem. Soc. Dalton Trans.*, (1993) 165. T.S.A. Hor, S.P. Neo, C.S. Tan, T.C.W. Mak, K.W.P. Leung and R.J. Wang, *Inorg. Chem., 31* (1992) 4510.
[7] L.T. Phang, T.S.A. Hor, Z.Y. Zhou and T.C.W. Mak, *J. Organomet. Chem., 469* (1994) 25. A. Houlton, D.M.P. Mingos, D.M. Murphy, D.J. Williams, L.T. Phang and T.S.A. Hor, *J. Chem. Soc. Dalton Trans.*, (1993) 3629.
[8] M.I. Bruce, P.A. Humphrey, O. bin Shawkataly, M.R. Snow, E.R.T. Tiekink and W.R. Cullen, *Organometallics, 9* (1990) 2910. M. Sato, H. Shigeta, M. Sekino and S. Akabori, *J. Organomet. Chem., 458* (1993) 199.
[9] W.Y. Yeh, S.B. Chen, S.M. Peng and G.H. Lee, *J. Organomet. Chem., 481* (1994) 183.
[10] W.H. Watson, A. Nagl, S. Hwang and M.G. Richmond, *J. Organometal. Chem., 445* (1993) 163.
[11] A.J. Downard, B.H. Robinson and J. Simpson, *J. Organomet. Chem., 447* (1993) 281. G. Balavoine, J. Collin, J.J. Bonnet and G. Lavigne, *J. Organomet. Chem., 262* (1984) 347. D.N. Duffy, M.M. Kassis and D.N. Rae, *Acta Crystallogr. Sect. C:, 47* (1991) 2054.
[12] Z.G. Fang, Y.S. Wen, R.K.L. Wong, S.C. Ng, L.K. Liu and T.S.A. Hor, *J. Cluster Sci., 5* (1994) 327.
[13] S. Onaka, M. Otsuka, A. Mizuno, S. Takagi, K. Sako and M. Otomo, *Chem. Lett.*, (1994) 45. S.M. Draper, C.E. Housecroft and A.L. Rheingold, *J. Organomet. Chem., 435* (1992) 9.
[14] J.T. Lin, S.Y. Wang, P.S. Huang, Y.M. Hsiao, Y.S. Wen and S.K. Yeh, *J. Organomet. Chem., 388* (1990) 151.
[15] C.J. McAdam, N.W. Duffy, B.H. Robinson and J. Simpson, submitted to *Organometallics*.
[16] D. Osella, C. Nervi, M. Ravera, N.W. Duffy, C.J. McAdam, B.H. Robinson and J. Simpson, *Inorg. Chim Acta, 247* (1995) 99.
[17] G. Pilloni, B. Longato and B. Corain, *J. Organomet. Chem., 420* (1991) 57.
[18] B.H. Robinson and J. Simpson, in M. Chanon (ed.), *Paramagnetic Organometallic Species in Activation / Selectivity, Catalysis*, Kluwer, Dordrecht, Netherlands, 1989, p. 357.
[19] C.M. Arewgoda, P.H. Rieger, B.H. Robinson, J. Simpson and S.J. Visco, *J. Am. Chem. Soc., 104* (1982) 5633.
[20] S.B. Colbran, B.H. Robinson and J. Simpson, *Organometallics, 2* (1983) 943; 952.
[21] B.H. Worth, B.H. Robinson and J. Simpson, *Organometallics, 11* (1992) 3863. S.M. Elder, B.H. Robinson and J. Simpson, *J. Organomet. Chem., 398* (1990) 165.
[22] D.M. Hoffman, R. Hoffmann and C.R. Fisel, *J. Am. Chem. Soc., 104* (1982) 3858.
[23] C.M. Arewgoda, B.H. Robinson and J. Simpson, *J. Am. Chem. Soc., 105* (1983) 1893.
[24] B.M. Peake, P.H. Rieger, B.H. Robinson and J. Simpson, *J. Am. Chem. Soc., 102* (1980) 156.
[25] G. Varadi, A. Vizi-Orosz, S. Vastag and G. Palyi, *J. Organomet. Chem., 108* (1976) 225. C.J. McAdam, N.W. Duffy, B.H. Robinson and J. Simpson, in preparation.
[26] D. Gregson and J.A.K. Howard, *Acta Crystallogr. Sect. C:, 39* (1983) 1024.
[27] J.-J. Bonnet and R. Mathieu, *Inorg. Chem., 17* (1978) 1973.
[28] C. Bianchini, P. Dapporto and A. Meli, *J. Organomet. Chem., 174* (1979) 205. R.G. Cunninghame, L.R. Hanton, S.D. Jensen, B.H. Robinson and J. Simpson, *Organometallics, 6* (1987) 1470.
[29] R.P. Aggarwal, N.G. Connelly, M.C. Crespo, B.J. Dunne, P.M. Hopkins and A.G. Orpen, *J. Chem. Soc. Dalton Trans.*, (1992) 655.
[30] A.J.M. Caffyn, M.J. Mays, G.A. Solan, D. Braga, P. Sabatino, G. Conole, M. McPartlin and H.R. Powell, *J. Chem. Soc. Dalton Trans.*, (1991) 3103.
[31] T.W. Matheson, B.H. Robinson and W.S. Tham, *J. Chem. Soc. A*, (1971) 1457. L.S. Chia, W.R. Cullen, M. Franklin and A.R. Manning, *Inorg. Chem., 14* (1975) 2521.
[32] P. Zanello, G. Opromolla, G. Giorgi, G. Sasso and A. Togni, *J. Organomet. Chem., 506* (1996) 61.
[33] B. Corain, B. Longato, G. Favero, D. Ajo, G. Pilloni, U. Russo and F.R. Kreissl, *Inorg. Chim. Acta, 157* (1989) 259.
[34] G. Pilloni and B. Longato, *Inorg. Chim. Acta, 208* (1993) 17.
[35] A.J. Downard, B.H. Robinson and J. Simpson, *Organometalics, 5* (1986) 1132.
[36] R.S. Dickson, B.M. Peake, P.H. Rieger, B.H. Robinson and J. Simpson, *J. Organomet. Chem., 172* (1979) C63. K. Hinkelmann, J. Heize, H.-T. Schect, J.S. Field and H. Vahrenkamp, *J. Am. Chem. Soc., 111* (1989) 5078.
[37] U. Kruerke and W. Hubel, *Chem. Ber., 94* (1961) 2829. J.L. Boston, D.W.A. Sharp and G. Wilkinson, *J. Chem. Soc.*, (1962) 3488.
[38] M.O. Nestle, J.E. Hallgren and D. Seyferth, *Inorg. Synth., 20* (1980) 226.
[39] J.J. Bishop, A. Davidson, M.L. Katscher, D.W. Lichtenberg, R.E. Merril and J.C. Smart, *J. Organomet. Chem., 27* (1971) 241.
[40] A.C. North, D.C. Philips and F.S. Mathews, *Acta Crystallogr. Sect. A:, 24* (1968) 351.
[41] G.M. Sheldrick, *A Program for the Solution of Crytal Structures from Diffraction Data*, University of Göttingen, Germany, 1986. G.M. Sheldrick, SHELXS-86, *Acta Crystallogr. Sect. A:, 46* (1990) 467.
[42] G.M. Sheldrick, SHELXL-93, *Program for Crystal Structure Refinement*, University of Göttingen, 1993.